# Activity and Stability of a Platinum Nanostructured Catalyst Deposited onto a Nitrogen-Doped Carbonaceous Support

**E. A. Moguchikh**[a, *]**, K. O. Paperzh**[a]**, A. A. Alekseenko**[a]**, E. N. Gribov**[b]**, and V. E. Guterman**[a]

[a] *Southern Federal University, Rostov-on-Don, Russia*
[b] *Novosibirsk State University, Novosibirsk, Russia*
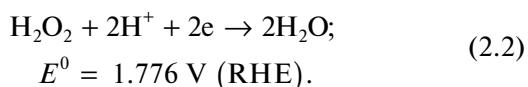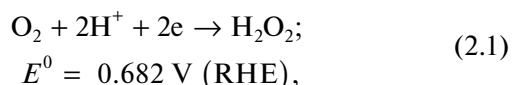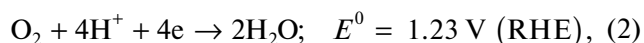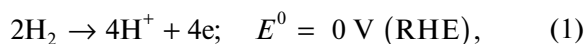***e-mail: liza.moguchix@mail.ru**

**Abstract**—A comparative analysis of the microstructure and electrochemical behavior of a platinum PCN catalyst synthesized over a nitrogen-doped carbon support and a commercial Pt/C-electrocatalyst HiSPEC3000 is carried out. The PCN catalyst is characterized by a smaller size of platinum nanoparticles and exhibits not only a higher activity in oxygen reduction reaction but also a higher corrosion-morphological resistance in acidic media.

## INTRODUCTION

Low-temperature fuel cells with proton-exchanging membranes are effective and environmentally-friendly systems for the chemical-to-electrical energy conversion. Electrochemical reactions occur therein at electrodes separated by membrane. Fuel (hydrogen, methanol, ethanol, or formic acid) is oxidized at anode [equation (1)], thus releasing electrons which migrate to cathode via external circuit. At the cathode, oxygen is electrochemically reduced to water [equation (2)]; the reaction has a complicated mechanism. It is recognized that this process includes different reaction paths, such as direct 4e-reduction of adsorbed oxygen to water [equation (2)]; 2e-reduction [equation (2.1)] to adsorbed $H_2O_2$ which then either is desorbed or is exerted to a secondary $2e^-$-reduction to water [equation (2.2)]. For example, the process occurring in a hydrogen–air fuel cell can be roughly presented as a sum of two half-reactions:

$$2H_2 \rightarrow 4H^+ + 4e; \quad E^0 = 0 \text{ V (RHE)}, \quad (1)$$

$$O_2 + 4H^+ + 4e \rightarrow 2H_2O; \quad E^0 = 1.23 \text{ V (RHE)}, \quad (2)$$

$$O_2 + 2H^+ + 2e \rightarrow H_2O_2; \\ E^0 = 0.682 \text{ V (RHE)}, \quad (2.1)$$

$$H_2O_2 + 2H^+ + 2e \rightarrow 2H_2O; \\ E^0 = 1.776 \text{ V (RHE)}. \quad (2.2)$$

The kinetics of the oxygen electroreduction reaction [equation (2)] are crucial for the effectiveness of the operation of fuel cells with proton-exchanging membrane. The low rate of the oxygen reduction reaction produced high overvoltage in the operating of oxygen electrode. It is well known that platinum-containing materials are the most active, widely used electrocatalysts for the oxygen reduction reaction [1, 2]. To increase the catalyst surface area, the platinum metal used to be converted to nanoparticles anchored at the support surface, most often, a carbonaceous one. The very usage of the platinum-containing catalysts hit up against a whole slew of difficulties. The platinum resources are limited, the prices in the platinum market are very high. In the fuel cell mass production, the cost of the catalyst may reach up to 50% of the cost of the fuel cell's membrane–electrode assembly [3]. One more problem is the Pt/C-catalyst insufficient stability. Under fuel cell operation, platinum dissolves, this is characteristic of small particles, the more so, nanoparticles. In addition, there occur nanoparticles agglomeration and the carbonaceous support degradation because of its oxidation by oxygen-containing intermediates. The carbonaceous support corrosion is also a source of the fuel cell catalytic layer degradation. The carbonaceous support for the fuel cell catalyst as such is thermodynamically unstable because of its low reversible potential: 0.207 V vs. reversible hydrogen electrode at 25°C [4]. This potential is lower than the cathode potential at the open circuit voltage (~1.0 V), hence, there is no thermodynamic factors preventing the carbon corrosion in the membrane–electrode assembly operation [5]. It was reported [6, 7] that the carbon support oxidation

occurred when the cathode potential exceeded 1.0 V vs. reversible hydrogen electrode. As to the reaction kinetics, the carbon corrosion rate is so small at potentials below 0.9 V that can be neglected. And yet, in the presence of Pt the carbon oxidation can occur even at the potential of 0.6 V [5, 8−10]. Under normal service conditions, the membrane−electrode assembly temperature approaches 65°C and the cathode local potential is below 0.9 V, so, the carbon corrosion rate is insignificant in virtue thereof [11]. However, during the fuel cell start/shutoff the amount of hydrogen in the near-anode space drops down dramatically [4, 11−14], which, in its turn, gives rise to the increase of the cathode potential up to 1.2 V and higher. This leads to the acceleration of the carbonaceous support corrosion. The fuel exhaustion at the anode is often connected with the presence of oxygen or the anode flooding. The matter is that membrane is not an ideal separator, and oxygen from the cathodic space can propagate through the membrane and accumulate during periods between the gas sequential passing. In addition, improper control of gas humidity in fuel cells can result in wrong distribution of the water flow and the electrode surface isolation.

The fuel cell restart after long halt used to result in the acceleration of the cathode corrosion, which favors structural changing [14]. In the fuel cell start, degradation of Pt per se is relatively small due to the high cathodic potential (over 1.0 V); by contrast, the carbon direct oxidation prevails. However, Pt can play the role of catalyst in the carbonaceous support corrosion. Nonetheless, the catalyst degradation mechanisms connected with the Pt oxidation to PtO or $PtO_2$ and their further dissolution in water as $Pt^{2+}$ should be taken into consideration in the evaluating of any strategy of the carbon corrosion prevention during the fuel cells' getting started [14]. The carbonaceous support oxidation resulted in the change of the porosity, loss of contact with some platinum nanoparticles, blocking of gas delivery to the platinum nanoparticles, weakening of the Pt-nanoparticles' adhesion and their further agglomeration. In addition, it can favor increase in the hydrophilic oxygen-containing groups' concentration at the carbonaceous support surface [11, 14], which aggravated problems connected with the flooding.

All above-described processes lower the catalyst activity [15−17]. Therefore, the development of stable nanomaterials combining small Pt content with high activity in the oxygen reduction reaction is a hot topic in the research destined to the increasing of the effectiveness of catalysts for fuel cells.

The most successive approaches to the increasing of the platinum-containing electrocatalysts' stability can be divided into three trends:

(1) optimization of the Pt/C-catalyst morphology with taking into consideration of the Pt-nanoparticles' size, form, and peculiarities of their distribution over the support surface [16−18];

(2) formation of highly active nanoparticles based on Pt−M bimetallic systems (M is the transition metal) with controlled architecture and composition [17−19];

(3) development of carbonaceous supports with elevated stability based on nanotubes, graphene, and graphitized carbonaceous materials, as well as carbonaceous supports doped with heteroatoms N, S, B, or F [11, 20]. Nitrogen-containing carbonaceous materials are studied most intensely.

Concerning the latter trend, it is necessary to distinguish between the using of the heteroatom-doped carbonaceous materials as platinum-less catalysts and their application as supports for the platinum nanoparticles. It was reported [2, 21] that porous carbons doped with heteroatoms (e.g., N, S, and P) showed electrocatalytical activity with respect to the oxygen reduction reaction. The matters is that the carbon doping with the heteroatoms affected the electron density distribution over its surface, hence, the material's catalytic activity [20, 21]. In the majority of papers devoted to the effects of nitrogen incorporated into the carbonaceous materials' structure these materials are used right as platinum-less catalysts in alkaline media. For catalytic areas with the N−C group, the carbon atom with the Lewis basicity neighboring a pyridine N atom considered being a catalytic center in acidic media [22]. Despite this, active N−C-centers demonstrated low activity and selectivity in the oxygen reduction reaction [21, 23, 24]. This resulted in high $H_2O_2$ yields. The using of C−N as individual catalytic system is likely to be impossible in acidic media.

The using of the nitrogen-doped carbonaceous materials as a platinum support in acidic media is studied but fragmentarily. Nonetheless, the prospects of these systems were demonstrated in many works. Because of the Pt catalytic effect on the carbon oxidation during long-term use of Pt/C-catalyst, the support degradation is accelerated with the increasing of the Pt : C ratio [21]. It is believed [21, 24] that the introducing of heteroatoms into the substrate structure favors lowering of the platinum aggressive action. According to works [20, 25], the metal deposition onto the nitrogen-doped carbon resulted in a well pronounced mutual isolation of the metal nanoparticles; and this is the reason of the increased catalyst stability against the acidic/alkaline corrosion and the prolongation of is service life. The introducing of N-atom into carbon layers makes the neighboring carbon atoms electron-deficient and decreased the gap between the conduction band and Fermi level, which leads to larger charge mobility [26, 27]. However, in all these studies too little emphasis is put on the role of the carbon modification when it is used as a support for the Pt-nanoparticle-based cathodic or anodic electrocatalysts in acidic media.

In this work, we performed a comparative study of a platinum electrocatalyst synthesized at an N-doped

**Table 1.** Composition and structural characteristics of the electrocatalysts

| Material | $S_{su}(C)$, $m^2/g$ | Platinum mass fraction, % | Platinum crystallite size, nm (XRD) | Platinum lattice parameter, Å | Nanoparticle average size, nm (TEM) |
|---|---|---|---|---|---|
| JM20 | $220 \pm 22$ | $20 \pm 2$ | $2.4 \pm 0.2$ | 0.3920 | $2.7 \pm 0.2$ |
| PCN | $250 \pm 25$ | $22 \pm 2$ | $0.8 \pm 0.2$ | 0.3968 | $1.9 \pm 0.2$ |

support and commercial Pt/C-catalyst JM20 (HiS-PEC3000, Johnson Matthey) concerning their activity in the oxygen reduction reaction and stability over different potential ranges in acidic electrolytes. The study is based on the hypothesis that the carbon support modification with nitrogen atoms can favor strengthening the adhesion of the deposited platinum nanoparticles to the support. This must have a positive effect on the catalyst stability and, probably, its activity in the oxygen reduction reaction.

## EXPERIMENTAL

### Synthesis of the Modified Support

The Ketjen black EC DJ-600 supports were modified with nitrogen after the procedure described in work [27]. In the experiment, acetonitrile was the nitrogen source. A support aliquot was charged to a quartz U-reactor. The reactor with the support was passed-through with argon saturated with the acetonitrile vapor at the room temperature for 4 h. The reactor temperature was 890°C; the flow rate, 0.4 cm³/s. The obtained material (in what follows, denoted as CN) contained 3.4 wt % of nitrogen; its surface area (after BET) is 250 m²/g. According to XPS data, the oxygen atom surface concentration in the modified support is about 2.8–3.6 at % [27]. The N/C ratio obtained by using XPS is equal to the bulk N/C-ratio obtained by CHN-analysis, and this points to the nitrogen uniform distribution over the entire bulk [27].

### Synthesis of the Pt/C−N-Electrocatalyst

The Pt/C−N-catalyst was synthesized by the platinum chemical reduction in $H_2PtCl_6 \cdot 6H_2O$ solution (*TU 2612-034-00205067–2003*) in the support-containing suspension. The support was a CN carbonaceous material. 0.15 g of the carbonaceous support was put into 18 mL of ethylene glycol (top-grade, purity no less than 99.8%, *GOST 19710–83*). The suspension was agitated using magnetic stirrer for 15 min, then homogenized for 1 min at the amplitude of 50%. Then, 6.64 mL of chloroplatinic acid solution [concentration 0.0179 g/mL ($H_2O$)] was added under constant agitation. After 5-min-agitation, 5.5 mL of 0.5 M NaOH solution was added, to set pH 10−11. The mixture was transferred into round-bottom 100-mL-flask. Then, 1 mL of formaldehyde (top-grade, concentration 37.2 wt %, *GOST 1625−89*) was added under constant agitation. Further, in the inert atmosphere the

temperature was elevated up to 80°C at which the reaction mixture was kept for 2 h under constant agitation. After spontaneous cooling of the suspension for 40 min, the product was filtered out, the filtered material was washed in sequence with portions of twice distilled water and isopropanol. The catalyst was oven-dried at 80°C for 1 h, then dried in desiccator over $P_2O_5$ for 12 h. In what follows, this product is denoted as PCN.

### Methods for Testing of the Materials' Composition and Structure

The platinum mass fraction in the catalyst was determined by the mass of the Pt-residue after the catalyst burning (800°C, 40 min). The measuring accuracy was ±3% (Table 1). The calculated platinum load in the PCN catalyst is 23 wt %. X-ray diffraction patterns of the Pt/C-materials were registered over the 2θ angle range from 15 to 55 grad using an ARL X'TRA diffractometer (Thermo Scientific, Switzerland), which used filtered Cu$K_\alpha$-radiation ($\lambda = 0.154056$ nm), at the room temperature. The X-ray diffraction patterns were processed by using a SciDavis software. The crystallite average size ($D_{av}$) was calculated by the Scherrer formula, basing on the characteristic (111) reflection, as described in work [28]. The $D_{av}$ determination accuracy is ±9% (Table 1).

The size of platinum nanoparticles in the PCN catalyst, their distribution in size and space was studied by transmission electron microscopy (TEM). The TEM-photographs were obtained by using a JEM-2100 microscope (JEOL, Japan) at a working voltage of 200 kV at a resolution of 0.2 nm. The TEM-photographs of the JM20 commercial sample were obtained by using a JEOL JEM-F200 microscope (at a voltage of 200 kV, current of 12−15 μA, CFEG) equipped with a cold field-emission electron gun.

In the measurements, 0.5 mg of the catalyst was added to 1 mL of isopropanol and dispersed by ultrasonication. A drop of the obtained suspension was applied to copper mesh coated by amorphous carbon and dried in air for 20 min at the room temperature. Histograms of the Pt-nanoparticles' distribution in size in the catalysts were plotted basing of the results of at least 400 randomly chosen particles in the TEM-images in the sample different spots.

**Table 2.** Parameters characterizing the catalysts' electrochemical behavior

| Material | Electrochemically active surface area, $m^2/g(Pt)$, $H_{ads}/H_{des}$ | $E_{1/2}$, V | $I_k$, A/g(Pt) | $I_k$, A/cm$^2$(Pt) |
|---|---|---|---|---|
| JM20 | $84 \pm 8$ | 0.91 | $184 \pm 18$ | $2.19 \pm 0.21$ |
| PCN | $110 \pm 11$ | 0.91 | $256 \pm 26$ | $2.33 \pm 0.24$ |

### Electrochemical Research Methods

Cyclic voltammogram were recorded at 25°C in a three-electrode cell filled with 0.1 M $HClO_4$ solution saturated with Ar at ambient pressure. Saturated silver/silver chloride electrode was the reference electrode; Pt-wire, the auxiliary electrode. Thin layer of Pt/C deposited onto a glassy carbon disc electrode was the working electrode. The procedure of the Pt/C preparation and deposition is described at length in work [17]. Prior to the electrode dipping into electrolyte solution, its surface was wetted with 0.1 M perchloric acid.

Primarily, we performed the electrochemical activation (standardizing) of the electrode surface. To that end, 100 cycles of the potential scanning was carried out over the potential range from 0.03 to 1.20 V (in this work, potentials are given vs. reversible hydrogen electrode) at a scanning rate of 200 mV/s. Further, two cyclic voltammograms were recorded in the same potential range, however, at a potential scanning rate of 20 mV/s. The catalyst electrochemically active surface area was determined from the half-sum of the charges consumed in the atomic hydrogen electrochemical adsorption/desorption during the recording of the 2nd cyclic voltammogram at a potential scanning rate of 20 mV/s, as described in work [17]. The accuracy of the electrochemically active surface area determination is ±10% (Table 2).

To determine the catalyst activity in the oxygen electroreduction reaction, we took a series of linear potential sweep voltammograms over the 0.0–1.20 V range at a potential scanning rate of 20 mV/s. Primarily, the cell was oxygen-saturated for 60 min at an electrode rotation velocity of 700 rpm. The Ohmic resistance contribution and the voltammogram normalization were carried out after generally accepted procedures described in works [29, 30]. The disc electrode rotation velocities were 400, 900, 1600, and 2500 rpm, as it is required for its activity determination by the kinetic current calculated from $I^{-1}-\omega^{-0.5}$ dependences (in the Koutecký–Levich coordinates) [31].

The catalysts' stability was evaluated by stress-testing based on the multiple voltametric potential cyclic sweeping at a rate of 100 mV/s: for 5000 cycles over the 0.6–1.0 V potential range and for 1000 cycles over the 0.6–1.4 V potential range. The stress-testing was carried out in the argon-saturated 0.1 M $HClO_4$ solution at 25°C. When 5000 cycles were performed, two cyclic voltammograms were recorded after each 500 cycles over the 0.02–1.20 V potential range at a potential scanning rate of 20 mV/s. In the stress-test with the 1000 cycles' duration, these two cyclic voltammograms were recorded after each 100 cycles. The electrochemically active surface area was calculated from the 2nd cyclic voltammogram, as described above [18].

### RESULTS AND DISCUSSION

The platinum mass fraction in the PCN sample synthesized from the nitrogen-doped carbon is 22 wt % (Table 1), which is close to the calculated value (23 wt %). This evidenced the support high sorption ability with respect to the metal nanoparticles.

The platinum crystallite average size in the PCN, calculated by the results of the X-ray diffraction analysis, does not exceed 1 nm (Table 1). The comparison of the X-ray diffraction patterns of the JM20 and PCN samples showed that in the PCN sample the carbon and platinum (111) reflections are shifted toward larger and smaller 2θ angle values, respectively (Fig. 1). It is our belief that the nitrogen heteroatoms built-in to the carbon crystal lattice affected its structural characteristics. The platinum nanoparticles' interaction with the heteroatoms can also affect the interatomic distance in the nanoparticles' crystal lattice. This was translated to a larger value of the platinum crystal lattice parameter in the PCN, as compared with that in JM20. In Table 1 we give the nanoparticles' average size and the elementary cell parameters determined by the mathematical processing with the use of the SciDavis software. We see from table that the platinum-nanoparticle elementary cell parameters for all samples are less than those in the platinum metal bulk. When the particles' average size decreased down to approximately 2 nm the elementary cell parameter decreased by 0.03 Å, which corresponds to a deviation by 0.7% as compared with the massive Pt. This could be understood as a result of the size effect being a consequence of uncompensated interatomic distances and reduced interplanar spacings near the particle surface. As a result, the nanoparticles shrink up which implies a decrease in the cell parameter [32].

TEM-microphotographs of the materials, containing the Pt-nanoparticle images, are presented in Fig. 2. The microphotographs of the JM20 sample (Fig. 2a) show nanoparticles sized from 1.5 to 4.5 nm, as well as separate aggregates containing comprising
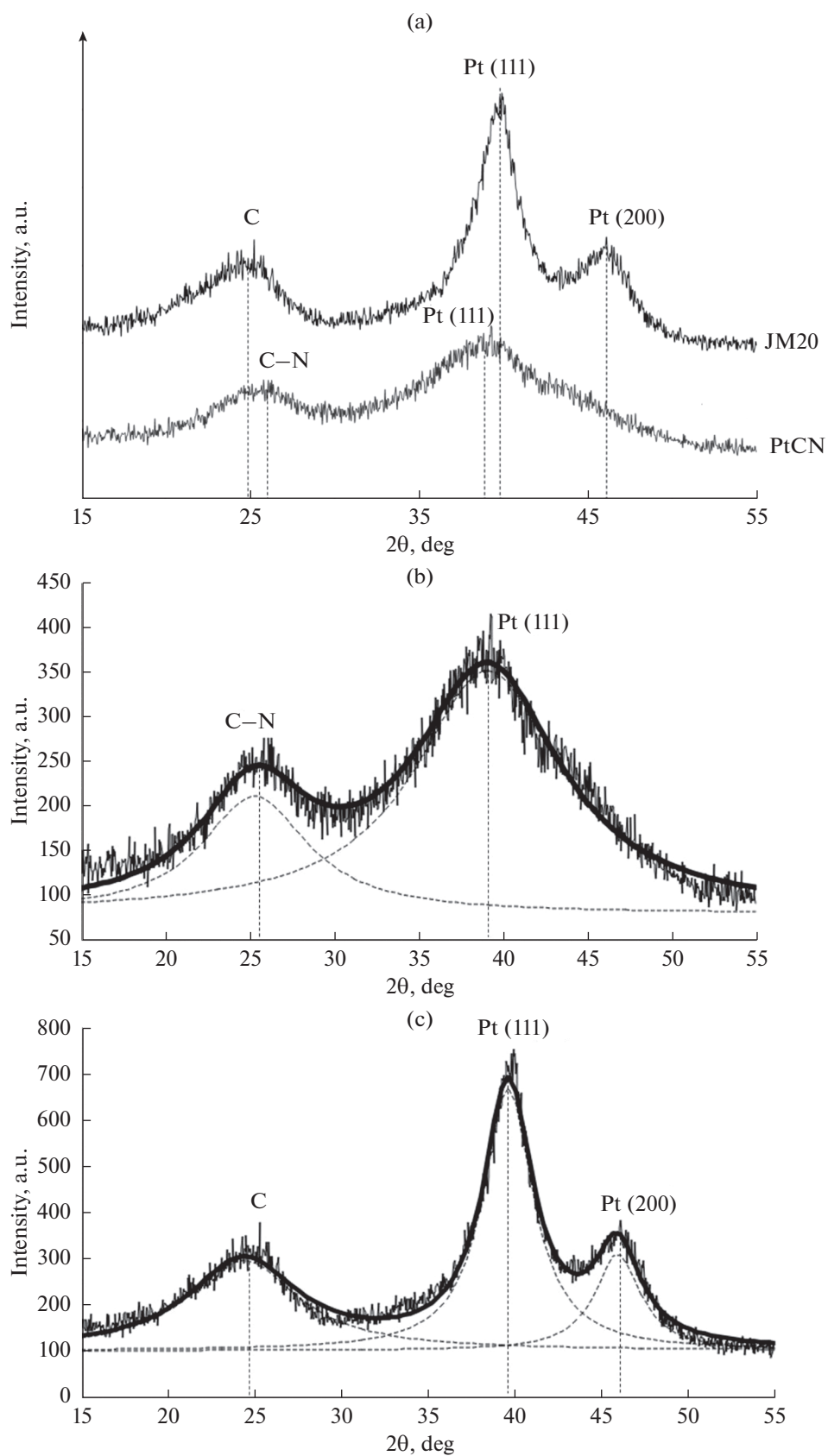
**Fig. 1.** X-ray diffraction patterns for Pt/C- and Pt/CN-electrocatalysts and schemes of the patterns' analysis for PCN (b) and JM20 (c).
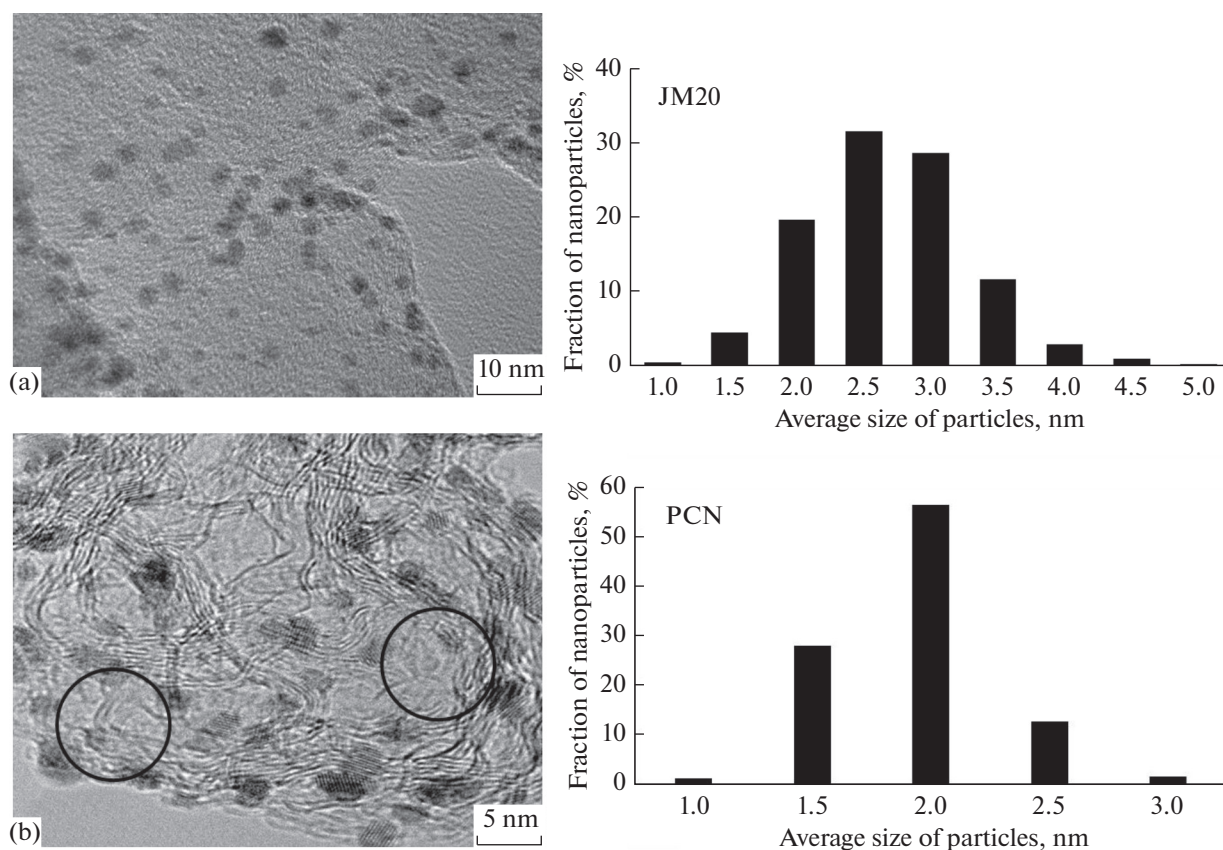
**Fig. 2.** TEM-microphotographs of the catalysts JM20 (a), PCN (b). Right—histograms of the nanoparticles' distribution in size in the corresponding materials.

2–4 particles. The nanoparticles' average size is 2.7 nm. In the catalyst prepared at a doped support the nanoparticles' average size is 1.9 nm (Fig. 2b). Their distribution in size is much narrower than in the commercial sample JM20. The platinum nanoparticles are distributed over the doped support more uniformly; at a closer study of PCN images (Fig. 2b) it can be observed that the considerable part of the nanoparticles is distributed along spherical trajectories. We believe that this can evidence the presence of mesopores whose edges could be thermodynamically attractive for the nanoparticles' nucleation and adhesion. Thus, the nature and morphology of the support material affected the Pt-nanoparticles' distribution.

In Table 1 we give details such as the studied catalysts' composition and microstructure, the carbonaceous supports' surface areas. Note that the carbonaceous materials used in both catalysts have surface areas close to each other.

During the stage of the catalyst suspension deposition onto the glassy carbon electrode surface we observed some difference in the lyophilic/lyophobic properties of the corresponding catalytic inks. The difference is retained also for the catalytic layers formed at the electrode. The PCN-catalyst layer appeared being more hydrophobic and was worse wetted by electrolyte. For this reason, the electrochemical standardizing of the PCN-catalyst surface, during which its active surface was developed, took as long as 90 cycles, whereas the commercial electrocatalyst JM20 surface appeared fully developed after only 30 cycles. We believe that the processes that can occur at the surface and in the bulk of the deposited PCN-catalyst porous layer in the course of multiple repeating of the cyclic voltammograms (see the Experimental section) could increase its hydrophily.

The form of cyclic voltammograms taken for the standardized catalysts are characteristic of Pt/C-materials (Fig. 3). The electrical double layer segment of the cyclic voltammograms, which corresponds to the electrical double layer charging processes over the 0.4–0.8 V potential range, is wider for PCN than for JM20. This correlates both with the specific surface area of the supports (Table 1) and with total surface area of the platinum nanoparticles in the catalysts (Table 2). Both catalysts demonstrated high values of the electrochemically active surface area; at that, in the PCN sample this area is larger by about 30% (Table 2). This well corresponds to the special features of the catalysts' microstructure: in PCN the platinum
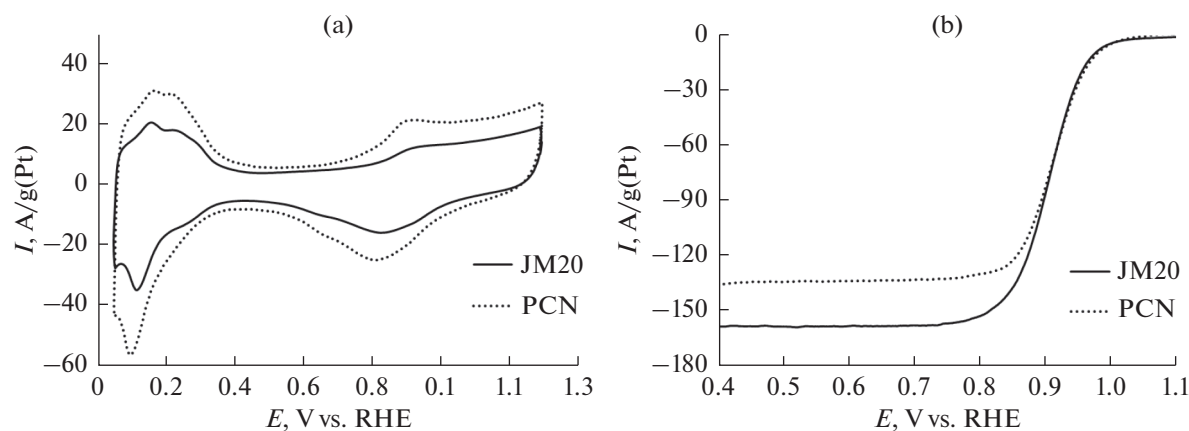
**Fig. 3.** Cyclic voltammograms of catalysts in Ar atmosphere (a), stationary electrode; voltammograms of electrocatalysts in $O_2$ atmosphere (b) at the rotating disc electrode, the rotation velocity 1600 rpm. Electrolyte 0.1 M $HClO_4$, potential scanning rate 20 mV/s.

nanoparticles are markedly smaller than in JM20 (Table 1).

The catalysts' activity was evaluated by their kinetic current and the oxygen electroreduction half-wave potential, which were measured at four rotation velocities of the rotating disc electrode: 400, 900, 1600, and 2500 rpm. Note that at all rotation velocities the PCN-catalyst showed lower limiting diffusion current of oxygen reduction than the JM20 one (Fig. 3b). This situation is likely to be due to some additional problems caused by oxygen diffusion in the PCN-catalyst porous layer because of the PCN lower hydrophily. Nonetheless, the PCN-electrocatalyst mass-activity ($I_k$, A/g(Pt)) in the oxygen reduction reaction appeared being much higher than that of the JM20-electrocatalyst (Table 2). Taking into consideration the negligibly small difference in the catalysts' activity in the oxygen reduction reaction ($I_k$, A/cm²(Pt)) (Table 2), it is the high electrochemically active surface area (due to the small size of the Pt-nanoparticles in the material) that should be considered to be the main reason of the PCN-catalyst larger mass-activity.

The durability of the catalysts was evaluated by way of multiple voltametric cycling in mild and hard mode over the potential ranges 0.6–1.0 V (5000 cycles) and 0.6–1.4 V (1000 cycles). According to literature data, the results of stress-testing in mild mode are mainly connected with the platinum dissolution–reprecipitation processes, its nanoparticles' aggregation, whereas the nature of carbonaceous support takes second place [18, 33, 34]. In the hard mode stress-testing, the support per se durability with respect to degradation is growing in importance [34]. Upon completing of the stress-testing, the stability was evaluated by the changing of the catalysts' electrochemically active surface area and mass-activity in the oxygen reduction reaction. In Figs. 4 and 5 we give the catalysts' cyclic voltammograms in argon atmosphere and voltammo-

grams of the oxygen electroreduction at the PCN and JM20 electrocatalysts prior to and after the corresponding stress-tests.

The catalysts' stress-testing in mild mode resulted in the current lowering in the "hydrogen" and, in a greater degree, "oxygen" segments of the cyclic voltammograms (Figs. 4a, 4c). The oxygen electroreduction voltammograms at pre-stress-tested electrodes are shifted toward the lower potential range (Figs. 4b, 4d), which evidenced deceleration of the oxygen reduction reaction. We note that after the stress-testing the PCN catalyst showed larger oxygen-reduction limiting diffusion current, which can be connected with the development (increase in hydrophily) of the porous catalytic layer deposited onto the rotating disc electrode.

The catalyst hard-mode stress-testing resulted in the current marked decrease both in the "hydrogen" and in "oxygen" segments of the cyclic voltammograms (Figs. 5a, 5c). At that, no broadening of the cyclic-voltammogram electrical double layer segment was observed during the cycling, which is an indirect evidence of the support stability against oxidation [18, 35]. The oxygen reduction reaction voltammograms are also shifted toward lower potentials (Figs. 5b, 5d). After 1000 cycles of the hard stress-testing, both catalysts demonstrated more significant decrease of the electrochemically active surface area (EASA) and mass-activity in the oxygen reduction reaction than after 5000 cycles of mild stress-testing (Fig. 6). In the hard mode, the electrochemically active surface area of the PCN catalyst dropped from 110 down to 40 m²/g(Pt); for the commercial catalyst JM20, from 84 down to 22 m²/g(Pt), which comes to 36 and 26%, respectively. The PCN and JM20 catalysts' mass-activity decreased after the stress-testing by a factor of 4.7 and 4.5, respectively (Fig. 6b). At that, the absolute value of the
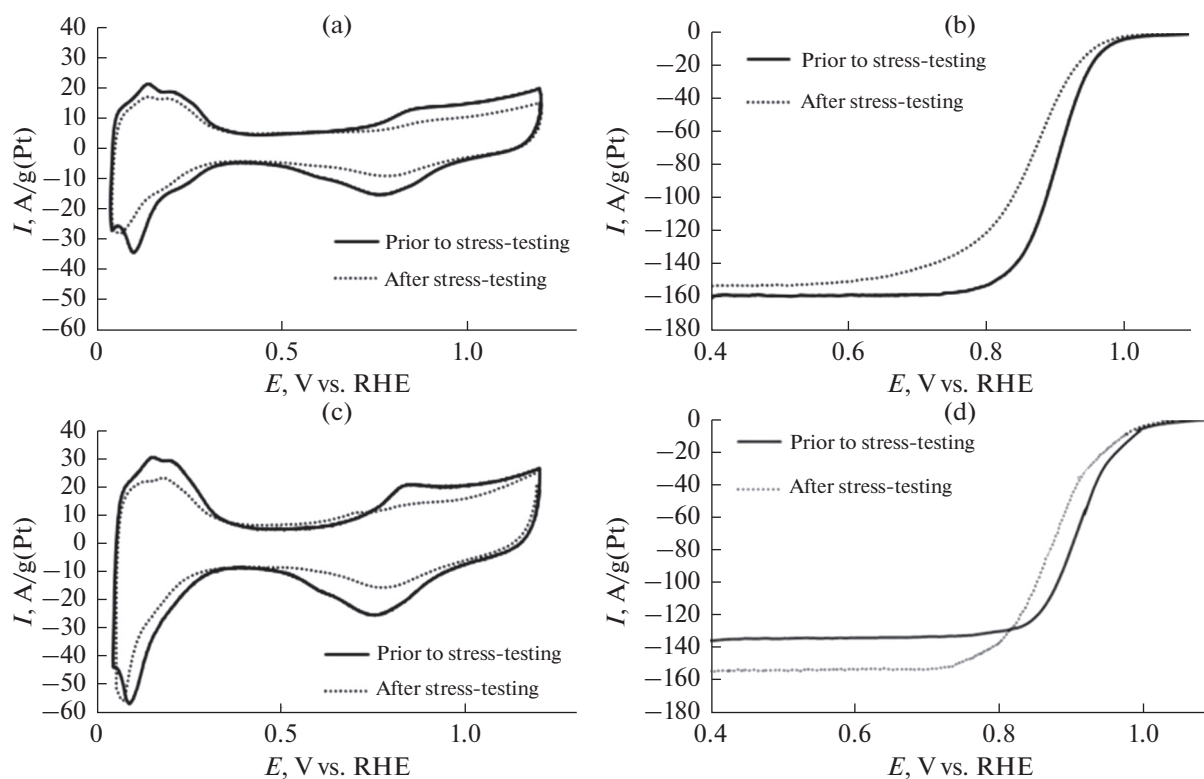
**Fig. 4.** Cyclic voltammograms of stationary electrodes in Ar atmosphere (a, c) prior to and after stress-testing. Voltammograms of oxygen electroreduction (b, d) prior to and after stress-testing at the rotating disc electrode rotation velocity of 1600 rpm. Catalysts: (a, b) JM20; (c, d) PCN. Electrolyte 0.1 M HClO$_4$. Potential scanning rate 20 mV/s. The stress-testing conditions: 5000 cycles over the 0.6−1.0 V potential range, 23°C.
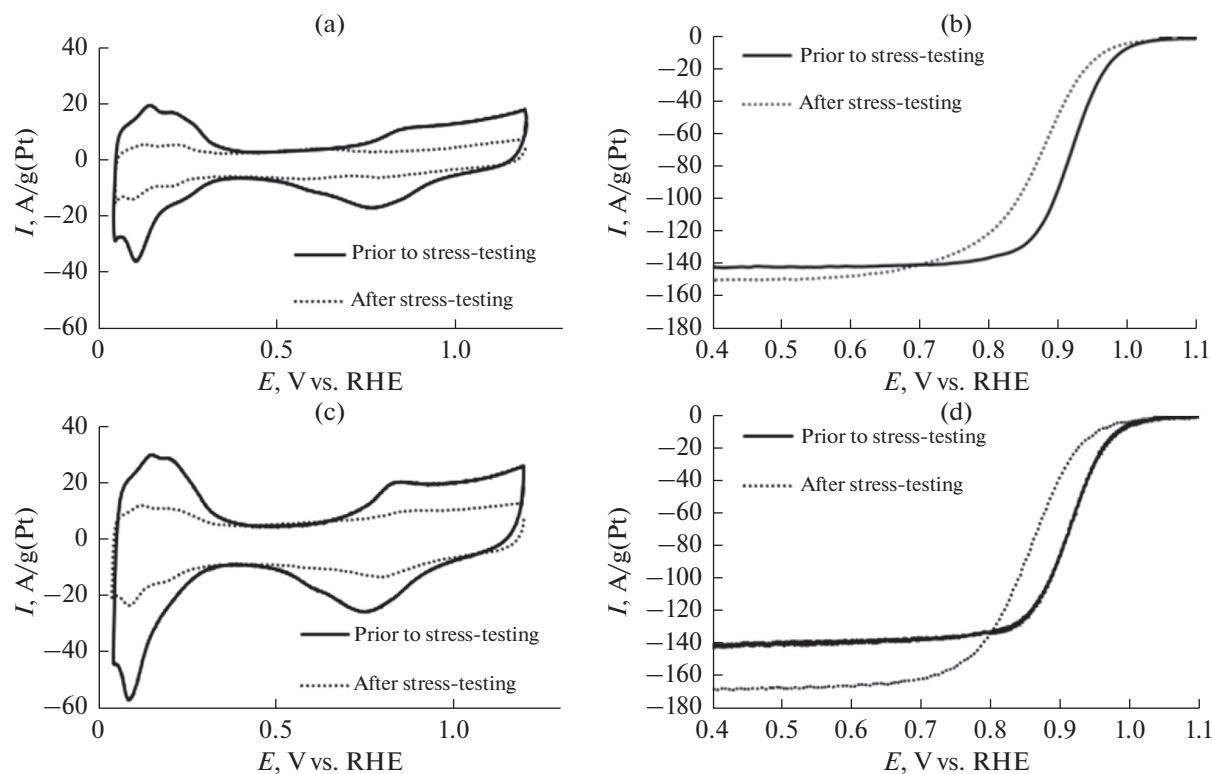


**Fig. 5.** Cyclic voltammograms of stationary electrodes in Ar atmosphere (a, c) prior to and after stress-testing. Voltammograms of oxygen electroreduction (b, d) prior to and after stress-testing at the disc rotation velocity of 1600 rpm. Catalysts: (a, b) JM20; (c, d) PCN. Electrolyte 0.1 M HClO$_4$. Potential scanning rate 20 mV/s. The stress-testing conditions: 1000 cycles over the 0.6−1.4 V potential range, 23°C.
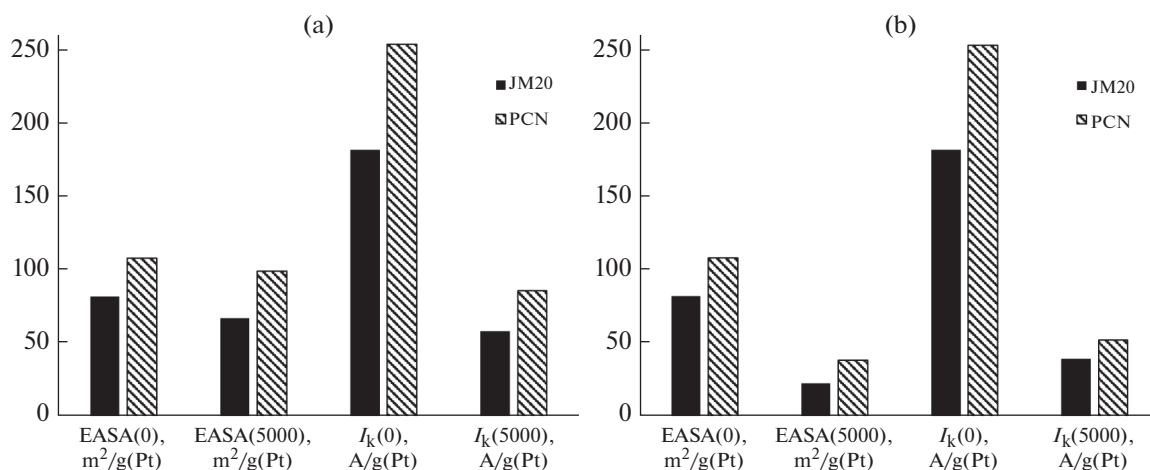
**Fig. 6.** Characteristic parameters of electrochemical behavior of Pt/C-catalysts prior to and after completing of stress-testing carried out in mild (a) and hard (b) modes. For additional explanation, see text.

PCN mass-activity still remained larger than that of JM20 (Fig. 6b).

The comparison of the catalysts' behavior in the course of the stress-testing in different modes allowed concluding on a higher PCN stability as compared with JM20. The nitrogen-doping of carbon is likely to strengthen the Pt-nanoparticle adhesion to the support, which hindered the platinum dissolution, hampered the nanoparticles' breaking-off or displacement along the support surface and thus prevented their aggregation during the stress-testing. One more factor increasing the sample stability can be the inherently larger support graphitization degree emerged during the carbonaceous materials high-temperature processing. And this, in its turn, resulted in a decrease of the number of oxygen-containing surface groups which take precedence in the oxidation during the catalysts' testing over wide potential range and contribute to the material degradation in total.

## CONCLUSIONS

A platinum catalyst PCN with the platinum mass fraction 22 wt % and the platinum nanoparticles average size 1.9 nm is synthesized in liquid phase using a nitrogen-doped carbonaceous support. Electronic interaction of the intercalated nitrogen atoms with carbon atoms and deposited platinum nanoparticles resulted in the shift of the carbon and platinum characteristic reflections in the material's X-ray diffraction patterns toward larger or smaller $2\theta$, angles, respectively. The platinum (111) reflections' position in the X-ray diffraction patterns allowed determining the platinum crystal lattice parameter: 0.3968 Å in the PCN nanoparticles; 0.3920 Å in the commercial Pt/C-catalyst JM20 nanoparticles.

The electrochemically active surface area of the PCN electrocatalyst and its mass-activity in the oxy-

gen reduction reaction appeared being larger than those of its commercial analog JM20. These differences are mainly due to the small size of the platinum nanoparticles in the PCN and well pronounced uniformity of their spatial distribution. The large electrochemically active surface area gives rise to the PCN high mass-activity in the oxygen reduction reaction, whereas specific activities of the PCN and JM20 catalysts are close to each other (they coincide within the limits of experimental error).

The catalysts' stability against degradation was evaluated in two modes of voltametric stress-testing. Despite smaller platinum nanoparticles' size, the PCN catalyst demonstrated higher stability in both stress-tests. Upon the completing of the testing, it retained its larger electrochemically active surface area and mass-activity in the oxygen reduction reaction as compared with the JM20.

We believe that the high stability of the PCN sample against degradation can be due to a combination of optimal morphology (uniformity of the Pt nanoparticles' spatial distribution and some special features of their arrangement in pores) and a positive impact from the nitrogen atoms incorporated to carbon on the strength of the platinum nanoparticles' adhesion to the support.

The platinum catalyst PCN synthesized on the nitrogen-doped carbon support is of apparent value for its testing in membrane—electrode assemblies of hydrogen—air fuel cells. We conceive the nitrogen-doped carbon material CN to be advantageous in the producing of two-component platinum-metal electrocatalysts as well.

CONFLICT OF INTEREST

The authors declare that they have no conflict of interest.


REFERENCES

1. Zhang, H., Hwang, S., Wang, M., Feng, Z., Karakalos, S., Luo, L., Qiao, Z., Xie, X., Wang, Ch., Su, D., Shao, Yu., and Wu, G., Single Atomic Iron Catalysts for Oxygen Reduction in Acidic Media: Particle Size Control and Thermal Activation, *J. Am. Chem. Soc.*, 2017, vol. 40, no. 139, p. 14143.
https://doi.org/10.1021/JACS.7B06514

2. Zheng, X., Wu, J., Cao, X., Abbott, J., Jin, C., Wang, H., Strasser, P., Yang, R., Chen, X., and Wu, G., N-, P-, and S-doped Graphene-like Carbon Catalysts Derived from Onium Salts with Enhanced Oxygen Chemisorption for Zn-air Battery Cathodes, *Appl. Catal. B: Environmental*, 2018.
https://doi.org/10.1016/J.APCATB.2018.09.054

3. Moriau, L.J., Hrnjic, A., Pavlisic, A., Kamsek, A.R., Petek, U., Ruiz-Zepeda, F., Sala, M., Pavko, L., Selih, V.S., Bele, M., Jovanovic, P., Gatalo, M., and Hodnik, N., Resolving the nanoparticles structure-property relationships at the atomic level: a study of Pt-based electrocatalysts, *iScience*, 2021, vol. 24, no. 2, 102102.
https://doi.org/10.1016/J.ISCI.2021.102102

4. Maillard, F., Simonov, P.A., and Savinova, E.R., *Carbon Materials as Supports for Fuel Cell Electrocatalysts*, *Carbon Mater. Catalysis*, 2008, p. 429.
https://doi.org/10.1002/9780470403709.CH12

5. Bentele, D., Aylar, K., Olsen, K., Klemm, E., and Eberhardt, S.H., PEMFC Anode Durability: Innovative Characterization Methods and Further Insights on OER Based Reversal Tolerance, *J. Electrochem. Soc.*, 2021, vol. 168, no. 2, p. 024515.
https://doi.org/10.1149/1945-7111/ABE50B

6. Stevens, D.A. and Dahn, J.R., Thermal degradation of the support in carbon-supported platinum electrocatalysts for PEM fuel cells, *Carbon*, 2005, vol. 43, p. 179.
https://doi.org/10.1016/J.CARBON.2004.09.004

7. Reiser, C.A., Bregoli, L., Patterson, T.W., Yi, J.S., Yang, J.D., Perry, M.L., and Jarvi, T.D., A Reverse-Current Decay Mechanism for Fuel Cells, *Electrochem. Solid-State Lett.*, 2005, vol. 8, p. A273.
https://doi.org/10.1149/1.1896466

8. Lee, G., Choi, H., and Tak, Y., In situ durability of various carbon supports against carbon corrosion during fuel starvation in a PEM fuel cell cathode, *Nanotech.*, 2018, vol. 30, no. 8, p. 085402.
https://doi.org/10.1088/1361-6528/aaf48c

9. Du, Y., Shen, Y.B., Zhan, Y.L., Ning, F.D., Yan, L.M., and Zhou, X.C., Highly active iridium catalyst for hydrogen production from formic acid, *Chinese Chem. Lett.*, 2017, vol. 28, p. 1746.
https://doi.org/10.1016/J.CCLET.2017.05.018

10. Castanheira, L., Silva, W.O., Lima, F.H.B., Crisci, A., Dubau, L., and Maillard, F., Carbon Corrosion in Proton-Exchange Membrane Fuel Cells: Effect of the Carbon Structure, the Degradation Protocol, and the Gas Atmosphere, *ACS Catal.*, 2015, vol. 5, p. 2184.
https://doi.org/10.1021/CS501973

11. Chen, J., Hu, J., and Waldecker, J.R., A Comprehensive Model for Carbon Corrosion during Fuel Cell Start-Up, *J. Electrochem. Soc.*, 2015, vol. 162, no. 8, p. F878.
https://doi.org/10.1149/2.0501508jes

12. Jia, F., Guo, L., and Liu, H., Dynamic characteristics of internal current during startups/shutdowns in proton exchange membrane fuel cells, *Int. J. Energy Res.*, 2019.
https://doi.org/10.1002/ER.4537

13. Tang, H., Qi, Z., Ramani, M., and Elter, J., PEM Fuel Cell Cathode Carbon Corrosion due to the Formation of Air/Fuel Boundary at the Anode, *J. Power Sources*, 2008, vol. 158, p. 1306.
https://doi.org/10.1016/j.jpowsour.2005.10.059

14. Meyer, Q., Pivac, I., Barbir, F., and Zhao, C., Detection of oxygen starvation during carbon corrosion in proton exchange membrane fuel cells using low-frequency electrochemical impedance spectroscopy, *J. Power Sources*, 2020, vol. 470, p. 228285.
https://doi.org/10.1016/J.JPOWSOUR.2020.228285

15. Messing, M. and Kjeang, E., Empirical modeling of cathode electrode durability in polymer electrolyte fuel cells, *J. Power Sources*, 2020, vol. 451, p. 227750.
https://doi.org/10.1016/J.JPOWSOUR.2020.227750

16. Alekseenko, A.A., Guterman, V.E., Belenov, S.V., Menshikov, V.S., Tabachkova, N.Y., Safronenko, O.I., and Moguchikh, E.A., Pt/C-electrocatalysts based on the nanoparticles with the gradient structure, *Int. J. Hydrog. Energy,* 2018, vol. 43, p. 3676.
https://doi.org/10.1016/J.IJHYDENE.2017.12.143

17. Guterman, V.E., Belenov, S.V., Alekseenko, A.A., Lin, R., Tabachkova, N.Y., and Safronenko, O.I., Activity and Stability of Pt/C and Pt–Cu/C Electrocatalysts, *Electrocatalysis*, 2018, vol. 9, p. 550.
https://doi.org/10.1007/s12678-017-0451-1

18. Yano, H., Watanabe, M., Iiyama, A., and Uchida, H., Particle-size effect of Pt cathode catalysts on durability in fuel cells, *Nano Energy*, 2016, vol. 29, p. 323.
https://doi.org/10.1016/J.NANOEN.2016.02.016

19. Polymeros, G., Baldizzone, C., Geiger, S., Grote, J.P., Knossalla, J., Mezzavilla, S., Keeley, G.P., Cherevko, S., Zeradjanin, A.R., Schüth, F., and Mayrhofer, K.J.J., High temperature stability study of carbon supported high surface area catalysts—expanding the boundaries of exsitu diagnostics, *Electrochim. Acta*, 2016, vol. 211, p. 744.
https://doi.org/10.1016/J.ELECTACTA.2016.06.105

20. Wanga, S., Wanga, H., Huang, Ch., Ye, P., Luo, X., Ning, J., Zhong, Y., and Hu, Y., Trifunctional electrocatalyst of N-doped graphitic carbon nanosheets encapsulated with CoFe alloy nanocrystals: The key roles of bimetal components and high-content graphitic-N,

*Appl. Catal. B: Environmental*, 2021, vol. 298, p. 120512.
https://doi.org/10.1016/J.APCATB.2021.120512GET

21. Cheng, J., Li, Yu., Huang, X., Wang, Q., Mei, A., and Kang, P., Shen Highly stable electrocatalysts supported on nitrogen-self-doped three-dimensional graphene like networks with hierarchical porous structures, *J. Mater. Chem. A*, 2015, vol. 3, p. 1492.
https://doi.org/10.1039/C4TA05552G

22. Wang, W., Jia, Q., Mukerjee, S., and Chen, S., Recent insights into the oxygen-reduction electrocatalysis of Fe/N/C materials, *ACS Catal.*, 2019, vol. 9, p. 10126.
https://doi.org/10.1021/ACSCATAL.9B02583

23. Imran Jafri, R., Rajalakshmi, N., and Ramaprabhu, S., Nitrogen doped graphene nanoplatelets as catalyst support for oxygen reduction reaction in proton exchange membrane fuel cell, *J. Mater. Chem.*, 2010, vol. 20, p. 7114.
https://doi.org/10.1039/C0JM00467G

24. Mardle, P., Ji, X., Wu, J., Guan, S., Dong, H., and Du, S., Thin film electrodes from Pt nanorods supported on aligned N-CNTs for proton exchange membrane fuel cells, *Appl. Catal. B: Environmental*, 2020, vol. 260, p. 118031.
https://doi.org/10.1016/J.APCATB.2019.118031

25. Hu, Y., Jensen, J.O., Zhang, W., Cleemann, L.N., Xing, W., Bjerrum, N.J., and Li, Q., Hollow spheres of iron carbide nanoparticles encased in graphitic layers as oxygen reduction catalysts, *Angew. Chem. Int. Ed.*, 2014, vol. 53, p. 3675.
https://doi.org/10.1002/ANIE.201400358

26. Wang, H., Ye, W., Yang, Y., Zhong, Y., and Hu, Y., Zn-ion hybrid supercapacitors: achievements, challenges and future perspectives, *Nano Energy*, 2021, vol. 85, p. 105942.
https://doi.org/10.1016/J.NANOEN.2021.105942

27. Golovin, V.A., Maltseva, N.V., Gribov, E.N., and Okunev, A.G., New nitrogen-containing carbon supports with improved corrosion resistance for proton exchange membrane fuel cells. International, *Int. J. Hydrog. Energy*, 2017, vol. 42, p. 11159.
https://doi.org/10.1016/J.IJHYDENE.2017.02.117

28. Langford, J.I. and Wilson, A.J.C., Scherrer after sixty years: A survey and some new results in the determination of crystallite size, *J. Appl. Crystallogr.*, 1978, vol. 11, no. 102.
https://doi.org/10.1107/S0021889878012844

29. Van der Vliet, D., Strmcnik, D.S., Wang, C., Stamenkovic, V.R., Markovic, N.M., and Koper, M.T.M., On the importance of correcting for the uncompensated Ohmic resistance in model experiments of the Oxygen Reduction Reaction, *J. Electroanal. Chem.*, 2010, vol. 647, p. 29.
https://doi.org/10.1016/J.JELECHEM.2010.05.016

30. Shinozaki, K., Zack, J.W., Pylypenko, S., Pivovar, B.S., and Kocha, S.S., Oxygen reduction reaction measurements on platinum electrocatalysts utilizing rotating disk electrode technique: II. Influence of ink formulation, catalyst layer uniformity and thickness, *J. Electrochem. Soc.,* 2015, vol. 162, p. F1384.
https://doi.org/10.1149/2.0551512JES

31. Pavlets, A., Alekseenko, A., Menshchikov, V., Belenov, S., Volochaev, V., Pankov, I., Safronenko, O., and Guterman, V., Influence of electrochemical pretreatment conditions of PtCu/C alloy electrocatalyst on its activity, *Nanomat.,* 2021, vol. 6, p. 1499.
https://doi.org/10.3390/NANO11061499

32. Leontyev, I.N., Kuriganova, A.B., Leontyev, N.G., Hennet, L., Rakhmatullin, A., Smirnova, N.V., and Dmitriev, V., Size dependence of the lattice parameters of carbon supported platinum nanoparticles: X-ray diffraction analysis and theoretical considerations, *RSC Adv.*, vol. 4, no. 68, p. 35959.
https://doi.org/10.1039/C4RA04809A

33. Riese, A., Banham, D., Ye, S., and Sun X., Accelerated stress testing by rotating disk electrode for carbon corrosion in fuel cell catalyst supports, *J. Electrochem. Soc.*, 2015, vol. 162, p. F783.
https://doi.org/10.1149/2.0911507JES

34. Testing Wang, C., Ricketts, M., Soleymani, A.P., Jankovic, Ja., Waldecker, J., and Chen, J., Effect of Carbon Support Characteristics on Fuel Cell Durability in Accelerated Stress *J. Electrochem. Soc.*, 2021, vol. 168, p. 044507.
https://doi.org/10.1149/2.0911507JES

35. Forouzandeh, F., Li, X., Banham, D.W., Feng, F., Ye, S., and Birss, V., Understanding the Corrosion Resistance of Meso- and Micro-Porous Carbons for Application in PEM Fuel Cells, *J. Electrochem. Soc.*, 2018, vol. 165, p. F3230.
https://doi.org/10.1149/2.0261806JES

*Translated by Yu. Pleskov*